Theory of x-ray scattering in high-pressure electrides

C. Fortmann,[1,2,*] C. Niemann,[1] and S. H. Glenzer[2]

[1]*Department of Physics and Astronomy, University of California Los Angeles, Los Angeles, California 90095, USA*

[2]*Lawrence Livermore National Laboratory, PO Box 808, L-493, Livermore, California 94551, USA*

(Received 8 June 2012; revised manuscript received 20 August 2012; published 29 November 2012)

We report on a theoretical model for the calculation of x-ray scattering from high-pressure electrides. By treating interstitial electrons as effective anions forming a sublattice within the crystal, we explicitly account for Bragg reflections from the sublattice as well as for scattering interferences between the ion lattice and the anion sublattice. The additional reflections and interferences lead to significant modifications of the static structure factor as compared to the pure lattices. Our results are important for accurate calculations of material properties in the high-pressure phase and allow for direct experimental verification of electride phases in matter at ultrahigh pressures through angle-resolved x-ray scattering.

DOI: 10.1103/PhysRevB.86.174116 PACS number(s): 61.05.cf, 61.50.Ks

Recent advances in dynamic shock-compression technology, using for example high-power lasers,[1] pinches,[2] or explosives,[3] allow us to study matter under extreme conditions of pressure (several 10–100 GPa), temperature (several 1000–10 000 K), and density (up to several 100 g/cm^3) over a vast range of parameters. An example is inertial confinement fusion (ICF) to reach conditions similar to the interior of the sun. Recent experiments have produced pressures of order 100 Gbars.[4] These high-pressure techniques produce near equilibrium states that are sufficiently long lived to investigate their thermodynamics using for example x-ray diagnostic techniques.

Single shock compression is limited to the principle Hugoniot[5] of the target matter, producing high-entropy states with temperatures of the order 1000 K, that is, above melting temperature for most materials. Multiple shock compression allows us to reach high-density states off the principal Hugoniot, that is, at lower temperature.[6,7] In the limit of isentropic ramp compression (i.e., infinitely many infinitesimally small shocks), dense crystalline matter below melting temperature is produced.

High-density, low-temperature solid phases have recently been investigated using modern *ab initio* computer simulation techniques, for example, density functional theory (DFT) combined with sophisticated structure finding tools.[8] In particular, the structure of simple metals under high pressure (several 10 to several 100 GPa) has received a lot of attention (e.g., lithium,[9] sodium,[10] potassium,[11] magnesium,[12] and Al[13]). Surprisingly, these studies showed that valence electrons, instead of becoming increasingly delocalized and Fermi degenerate, as one might naively expect, pair and localize in interstitial cages formed by the still persisting ion lattice.[14,15] This phenomenon is explained in terms of Coulomb repulsion between valence and core electrons and orthogonality between these states. It was also found that these systems still exhibit metallic or semimetallic conductivity, which is related to the relatively high-kinetic energy of electrons within the interstitial cages and interaction effects between the Brillouin zone boundary and the Fermi edge.[13,16]

The existence of such "electride" states of matter was known previously only from certain complex organic and inorganic compounds (see, e.g., Ref. 17). Indirect evidence for high-pressure electride states in Li were observed,[18] that is, a drop in the conductivity above 65 GPa associated with the strong electron localization and structural phase transition that was predicted in the same pressure regime.[9]

A direct observation of the electride character of high-pressure, low-temperature solids is still missing. In this paper we demonstrate that angle-resolved x-ray Thomson scattering (XRTS) can prove the existence of high-pressure electride phases if the sublattice of interstitial electrons exhibits a different space symmetry than the ion lattice. This is the case, for example, for Mg at 500 GPa. In other cases (e.g., Li at 85 GPa) we predict a significant change in scattering intensity at characteristic scattering angles, pointing to but not proving unambiguously the presence of electride states.

We develop a model for the structure factor $S(\vec{k})$ for electrides. The model is applied to calculate the x-ray scattering profile for the predicted electride structures of lithium (Li) and magnesium (Mg) at high pressure and room temperature. In the case of Li, various structural phase transitions were observed experimentally[19] at pressures ranging in the multi ten GPa range, i.e., well accessible in static compression experiments. Quantum molecular dynamics simulations[9] support the observed structures and also predict strong electron localization, for example, in the Li oc40 phase, which is stable between 65 and 95 GPa. As a second example we consider Mg, which was predicted to undergo a sequence of phase transitions between various electride structures in the multi hundred GPa range.[12] Between ∼500 and 756 GPa, fcc is found to be the most stable crystal structure. In the simulations, valence electrons were shown to localize in the interstitial cages, forming a simple cubic (sc) sublattice. Precisely this sublattice leads to unmistakable features in the scattering profile and thus provides a criterion to experimentally demonstrate the existence of the electride phase: A pure fcc lattice (i.e., without localized interstitial electrons) is characterized by systematic absences at the (100) and (110) Bragg reflections. The interstitial electron sublattice is of sc type and hence shows Bragg peaks at these positions. Above 756 GPa the structure transitions to a simple hexagonal (sh) phase with interstitial electrons between the honeycomb lattices. Here, interference between electride and ion lattices alters the peak intensities of the (100) and (110) reflection significantly.

Angle-resolved high-energy x-ray scattering experiments will directly measure the new structure peaks from electrides. For example, electride experiments in millimeter-scale magnesium samples can be approached in static high-pressure diamond anvil cell[20] or in dynamic compression experiments on high-power lasers.[21] The latter approach is principally capable of producing pressures exceeding those required for producing electrides and further allow dynamic probing with laser-produced Mo K-shell radiation at 18 keV. These plasma x-ray sources provide sufficient photons for single shot observations with high-photon energy that are required to penetrate through mid-Z material. Also free-electron lasers may provide the required x-ray probe capability,[22,23] particularly when using high harmonics.

During the x-ray scattering process, the incident photon transfers momentum $\hbar\vec{k} = 2E_0/\hbar c \sin(\theta/2)$. Thus, the scattering geometry and the probe energy determine the scale length $\propto 1/k$ of the electron density fluctuations measured in the scattering experiment.

Observing the Mg (100) peak with $k_{100} = 30$ nm^{-1} and $E = 18$ keV requires forward scattering at $\theta = 20^\circ$. For a He-α bandwidth of $\Delta E/E = 2 \times 10^{-2}$ and angular resolution of $\Delta\theta/\theta = 0.25$ we find $\Delta k/k \simeq 0.25$ sufficient to isolate the additional (100) and (110) peaks.

Interstitial electrons act as anions[17] and are treated as additional centers of the primitive cell. The scattering profile, that is, the absolute scattered intensity as function of scattering angle, will be dominated by narrow peaks corresponding to Bragg reflections from the lattice planes. We write the x-ray scattering cross section as

$$\frac{d\sigma}{d\Omega} = \sigma_{\mathrm{Th}} S(\vec{k}). \tag{1}$$

Here $S(\vec{k})$ is the electron structure factor given by the Fourier transform of the electron-electron pair correlation function. It can be written as[24]

$$S(\vec{k}) = e^{-2W(k)} \frac{(2\pi)^3}{n_e} \sum_{\vec{G}\neq 0} |n_{e\vec{G}}|^2 \delta(\vec{k} - \vec{G}) + [1 - e^{-2W(k)}]. \tag{2}$$

The first term describes coherent (Bragg) scattering from lattice planes characterized by inverse lattice vectors $\vec{G}$. Their amplitude is given by the Fourier component of the electron density

$$n_{e\vec{G}} = \sum_i f_i \exp(-i\vec{G}\cdot\vec{d}_i), \tag{3}$$

which coherently sums scattering amplitudes from all sites within the lattice basis $\{\vec{d}_i\}$; $f_i(k)$ is ionic form factor. The Debye-Waller factor $\exp[-2W(k)]$ accounts for the reduction in intensity due to thermal lattice vibrations. Correspondingly, thermal diffuse (incoherent) scattering is described through the second term in Eq. (2). Within the Debye model for cubic lattices,[25]

$$W(k) = \frac{3}{4k_{\mathrm{B}}T_D}\frac{\hbar^2k^2}{2m_I}\left[1 + 4\left(\frac{T}{T_D}\right)^2 \int_0^{T/T_D} \frac{x\,dx}{e^x - 1}\right]. \tag{4}$$

For simplicity we assume that interstitial electrons adiabatically follow the ion lattice vibrations, hence only one Debye-Waller factor appears to describe the thermal motion for both lattice ions and interstitial sites; T_D is the Debye temperature.

After separating the electron density $n_{e\vec{G}}$ into core electrons centered around lattice ions (I) and interstitial electrons (X) $n_{e\vec{G}} = n_{I\vec{G}} + n_{X\vec{G}}$, we can rewrite Eq. (2) as

$$\begin{aligned} S(\vec{k}) &= e^{-2W(k)}(2\pi)^3 \sum_{\vec{G}\neq 0} \left| f_I(\vec{k}) \sum_{\text{ionsites}} \exp(-i\vec{k}\cdot\vec{d}_i) + f_X(\vec{k}) \sum_{\text{interst.}} \exp(-i\vec{k}\cdot\vec{d}_i) \right|^2 \delta(\vec{k} - \vec{G}) + [1 - e^{-2W(k)}] \\ &= e^{-2W(k)}(2\pi)^3 \{ |f_I(\vec{k})|^2 S_{ii}(\vec{k}) + |f_X(\vec{k})|^2 S_{xx}(\vec{k}) + 2\mathrm{Re}\,[f_I(\vec{k}) f_X^*(\vec{k})] S_{xi}(\vec{k}) \} + [1 - e^{-2W(k)}], \end{aligned} \tag{5}$$

$f_I(\vec{k})$ is the core electron form factor and $f_X(\vec{k})$ is the interstitial electron form factor. In the absence of interstitial electrons $f_X(\vec{k}) = 0$ one finds the usual expression for coherent scattering from pure ion lattices.[24] Scattering interferences between lattice ions and electride anions (electrons) are taken into account via the "mixed" structure factor $S_{xi}(\vec{k})$. This interference term alters the peak amplitudes when compared to the pure ion lattice. Additional peaks appear when the electride sublattice belongs to a different space symmetry group than the ion lattice.

As a first application we calculate the electron structure for Li at ~85 GPa pressure. Lattice parameters and symmetry groups are taken from Ref. 9. The length of the basis vectors of the primitive cell are $a = 0.4942$ nm, $b = 0.8026$ nm, and $c = 0.6784$ nm. Electrons are predicted to localize in three basins within the unit cell with the electron localization function (ELF) taking on values of 0.9 and higher. The ELF measures the density distribution of electron pairs and is normalized such that ELF $\leqslant 1$. For simplicity we approximate the interstitial electron density by a spherically symmetric Gaussian distribution. Results for the partial structure factors and the sum over all contributions are shown in Fig. 1(a) as function of the transfer wave vector k. It is clearly seen how the presence of interstitial electrons alters the amplitude of the first Bragg peak at $k = 7.8$ nm^{-1} (010): All three contributions are positive and add up, making this peak twice as intense as the second peak at 12.7 nm^{-1} (100). In contrast, assuming a pure ion lattice, represented by the black curve, both peaks are of approximately the same intensity. Here scattering from the electride lattice (blue curve) and the interference terms (red curve) nearly cancel each other; the peak intensity dominated by the ion lattice term. The factor 2 difference in peak intensity

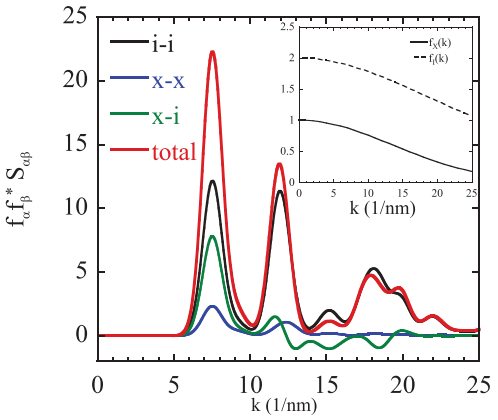

FIG. 1. (Color online) Partial structure factors for Li at 85 GPa pressure showing contributions from the ionic lattice (black curve), interstitial electrons (blue curve), and the interference term (green). The sum of all terms is shown as the red curve. The inset shows the ionic form factors for lattice ions (I) and interstitial sites (X).

should be clearly detectable in an experiment as proposed in this paper. It points towards existence of an electride structure, but is not a definite proof, as other effects like disorder and especially anisotropies at high pressure could also lead to this observation. Experimental diffraction data for Li at 86 GPa exists[26] but low signal-to-noise ratio prohibits extraction of Bragg intensities and comparison to our model.

More striking differences between the pure ion lattice and the electride structure that are unambiguously attributable to electride behavior are found in Mg. The pressures to reach these structures are by a factor of 10 larger compared to the Li case and can presently not be achieved by static compression. Dynamic compression using a ramp compression strategy to keep the entropy production and heating low will have to be applied. Electron structure factors for magnesium at pressures between 500 and 800 GPa are shown in Fig. 2. Lattice structure parameters (space symmetry group, dimensions of the unit cell, and coexistence curves) are taken from Ref. 12. These simulations predict that Mg undergoes a structural phase transition from bcc to fcc at 456 GPa pressure at room temperature.[12] The length of the primitive lattice vectors in the fcc phase is $a = 2.1$ Å. The electron localization function (ELF)[27] assumes maximum values of $\sim$0.91 in the eight interstitial spaces of the fcc primitive cell, forming a simple cubic (sc) lattice. Zeros in the ELF mark the spatial extension of the interstitial electron cloud.

The total structure factor and the three partial structure factors $|f_I|^2 S_{ii}(k), |f_X|^2 S_{xx}(k)$, and $2\mathrm{Re}\,[f_I f_X^*] S_{xi}(k)$ are shown in Fig. 2(a). The structures are averaged over all lattice orientations, thus representing scattering from a polycrystalline sample. The bottom x axis shows the wave number k in units of the reciprocal lattice spacing $k_0 = 2\pi/a = 30\ \mathrm{nm}^{-1}$, the top x axis shows k in units of 1/nm. The lattice peaks are represented by narrow Gaussians. The total structure factor has an offset of +50 for better discernibility from the partial structure factors. The fcc ion lattice (black line) is characterized by systematic absences at the (100) ($k = k_0 = 30\ \mathrm{nm}^{-1}$) and (110) ($k = \sqrt{2}k_0 = 42\ \mathrm{nm}^{-1}$) position. Here the interstitial sc lattice produces notable signals. The (111) peak ($k = \sqrt{3}k_0 = 52\ \mathrm{nm}^{-1}$) is slightly amplified with respect to the pure fcc lattice peak (S_{ii}) due to the interference term S_{xi} and to a small extent from electron lattice scattering. Beyond $k = 2k_0 = 60\ \mathrm{nm}^{-1}$, the interstitial form factor $f_X(k)$ practically vanishes and sc lattice and interference terms are suppressed. The form factors are shown in the inset in Fig. 2(a).

Figure 2(b) shows the total scattering profile for fcc Mg with (red) and without (black) interstitial electrons, taking into account the Debye-Waller factor and the incoherent contribution (shown in the inset). Bragg peaks at (100) and (110) positions in the electride phase are clearly identified.

At 756 GPa, Mg transitions to the simple hexagonal (sh) phase with interstitial electrons between the honeycomb

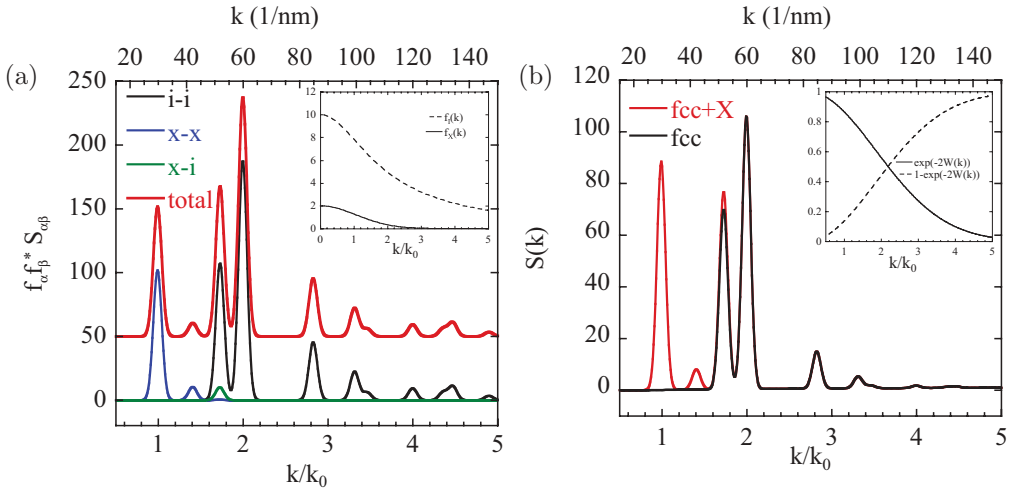

FIG. 2. (Color online) (a) Structure of Mg at 500 GPa: Partial and total static structure factors for the fcc electride lattice. The inset shows the form factors for lattice ions (dashed) and interstitial electrons (solid). (b) Total structure factor for Mg for fcc lattice shows the appearance of a strong (100) peak along with weak contributions at the (110) and (111) positions (red curve). Black curve is fcc without interstitial electrons. The inset shows the Debye-Waller functions that describe the decay in Bragg intensity due to thermal lattice vibrations (solid line) and the amount of thermal diffuse scattering (dashed).

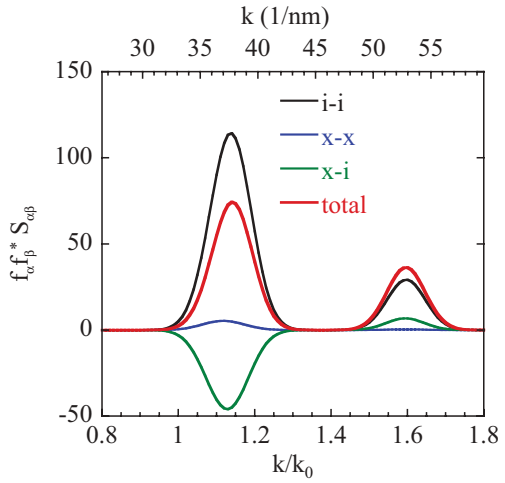

FIG. 3. (Color online) Static structure factors for Mg at 800 GP.

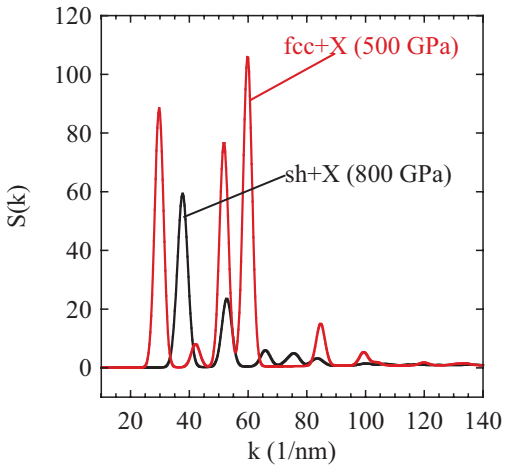

FIG. 4. (Color online) Scattering profiles for fcc and sh electride phases in Mg at ultrahigh pressures.

lattices. The lattice dimensions are $a = 0.189$ nm and $c = 0.9a$. The total structure factor and the partial structure factors are shown in Fig. 3. No additional reflections are observed in the total structure compared to the ion-ion structure. Instead, being of the same order as $S_{ii}(k)$, the interference term $S_{xi}(k)$ strongly affects the total signal. In the vicinity of the first Bragg peak ($k = 37.5$/nm), the interference term is negative, hence this peak is reduced in intensity by ∼30%. Conversely, the second peak is slightly enhanced through the interference term by ∼10%. These changes in the peak amplitude are again indicating the presence of interstitial electrons, although not as unmistakable as in the case of the fcc phase since variations in peak intensities of the order 10% can also be attributed to other effects like disorder or thermal lattice vibrations (Debye-Waller effect). As an advantage of this technique, no absolute intensity measurement is required. As a further observation, we note that the sh electride structure is greatly different from the lower pressure fcc electride structure as can be seen in Fig. 4. Due to higher compression, the position of the first correlation peak is shifted to higher wave numbers. Also, the coordination number is decreased from 12 to 8 and the number of ions per unit cell is reduced from 4 to 1 when going from fcc to sh phase, explaining the drop in overall intensity between both phases. Hence, observation of the location of the low k peaks and the overall scattering intensities will enable us to observe the phase transition between fcc and sh phase predicted at 756 GPa.

In conclusion, we have presented a model for the calculation of static structure factors for high-pressure electride systems. Application of the model to predicted high-pressure structures for Li and Mg have shown that angle-resolved scattering of multi-keV x rays is a strong candidate to demonstrate the existence of electride phases in statically compressed or ramp compressed targets in a clear-cut way. In Li, the oc40 phase with interstitials that is predicted for pressures of 85 GPa will result in a 50% change in the first correlation peak amplitude when including the interstitial electrons. Other effects, especially anisotropy, would have to be excluded to make a definite conclusion about the presence of electrides. Second, appearance of additional correlation peaks in the fcc phase of Mg are the most obvious indications for electrides pointing towards a decisive experiment with pulsed high-power lasers to verify high-pressure electride phases.

This work was performed under the auspices of the US Department of Energy by Lawrence Livermore National Laboratory under Contract No. DE-AC52-07NA27344 and supported by LDRD Grant No. 10-ER-050. C.F. acknowledges support by the Alexander von Humboldt Foundation.

*carsten.fortmann@zoho.com

[1] J. D. Lindl, P. Amendt, R. L. Berger, S. G. Glendinning, S. H. Glenzer, S. W. Haan, R. L. Kauffman, O. L. Landen, and L. J. Suter, Phys. Plasmas **11**, 339 (2004).

[2] M. K. Matzen *et al.*, Phys. Plasmas **12**, 055503 (2005).

[3] V. E. Fortov, R. I. Ilkaev, V. A. Arinin, V. V. Burtzev, V. A. Golubev, I. L. Iosilevskiy, V. V. Khrustalev, A. L. Mikhailov, M. A. Mochalov, V. Y. Ternovoi, and M. V. Zhernokletov, Phys. Rev. Lett. **99**, 185001 (2007).

[4] S. H. Glenzer *et al.*, Phys. Plasmas **19**, 056318 (2012).

[5] Y. B. Zel'Dovich and Y. P. Raizer, *Physics of Shock Waves and High-Temperature Hydrodynamic Phenomena*, edited by W. D. Hayes and R. F. Probstein (Dover, New York, 2002).

[6] J. Hawreliak, J. Colvin, J. Eggert, D. Kalantar, H. Lorenzana, S. Pollaine, K. Rosolankova, B. Remington, J. Stölken, and J. Wark, Astrophys. Space Sci. **307**, 285 (2007).

[7] A. L. Kritcher, P. Neumayer, J. Castor, T. Döppner, R. W. Falcone, O. L. Landen, H. J. Lee, R. W. Lee, E. C. Morse, A. Ng, S. Pollaine, D. Price, and S. H. Glenzer, Science **322**, 69 (2008).

[8] C. J. Pickard and R. J. Needs, Phys. Rev. Lett. **97**, 045504 (2006).

[9] M. Marqués, M. I. McMahon, E. Gregoryanz, M. Hanfland, C. L. Guillaume, C. J. Pickard, G. J. Ackland, and R. J. Nelmes, Phys. Rev. Lett. **106**, 095502 (2011).

[10] M. Marqués, M. Santoro, C. L. Guillaume, F. A. Gorelli, J. Contreras-García, R. T. Howie, A. F. Goncharov, and E. Gregoryanz, Phys. Rev. B **83**, 184106 (2011).

[11]M. Marqués, G. J. Ackland, L. F. Lundegaard, G. Stinton, R. J. Nelmes, M. I. McMahon, and J. Contreras-García, Phys. Rev. Lett. **103**, 115501 (2009).
[12]P. Li, G. Gao, Y. Wang, and Y. Ma, J. Phys. Chem. C **114**, 21745 (2010).
[13]C. J. Pickard and R. J. Needs, Nat. Mater. **9**, 624 (2010).
[14]J. B. Neaton and N. W. Ashcroft, Nature (London) **400**, 141 (1999).
[15]Y. Ma, M. Eremets, A. R. Oganov, Y. Xie, I. Trojan, S. Medvedev, A. O. Lyakhov, M. Valle, and V. Prakapenka, Nature (London) **458**, 182 (2009).
[16]H. Jones, Proc. R. Soc. London A **147**, 396 (1934).
[17]J. L. Dye, Science **247**, 663 (1990).
[18]T. Matsuoka and K. Shimizu, Nature (London) **458**, 186 (2009).
[19]C. L. Guillaume, E. Gregoryanz, O. Degtyareva, M. I. McMahon, M. Hanfland, S. Evans, M. Guthrie, S. V. Sinogeikin, and H.-K. Mao, Nat. Phys. **7**, 211 (2011).
[20]H.-K. Mao and R. J. Hemley, Rev. Mod. Phys. **66**, 671 (1994).
[21]S. H. Glenzer and R. Redmer, Rev. Mod. Phys. **81**, 1625 (2009).
[22]R. W. Lee, S. J. Moon, H.-K. Chung, W. Rozmus, H. A. Baldis, G. Gregori, R. C. Cauble, O. L. Landen, J. S. Wark, A. Ng, S. J. Rose, C. L. Lewis, D. Riley, J.-C. Gauthier, and P. Audebert, J. Opt. Soc. Am. B **20**, 770 (2003).
[23]S. P. Hau-Riege, A. Graf, T. Döppner, R. A. London, J. Krzywinski, C. Fortmann, S. H. Glenzer, M. Frank, K. Sokolowski-Tinten, M. Messerschmidt, C. Bostedt, S. Schorb, J. A. Bradley, A. Lutman, D. Rolles, A. Rudenko, and B. Rudek, Phys. Rev. Lett. **108**, 217402 (2012).
[24]D. A. Baiko, A. D. Kaminker, A. Y. Potekhin, and D. G. Yakovlev, Phys. Rev. Lett. **81**, 5556 (1998).
[25]C. Kittel, *Quantum Theory of Solids* (Wiley, New York, 1963).
[26]T. Matsuoka, S. Onoda, M. Kaneshige, Y. Nakamoto, K. Shimizu, T. Kagayama, and Y. Ohishi, J. Phys.: Conf. Ser. **121**, 052003 (2008).
[27]A. D. Becke and K. E. Edgecombe, J. Chem. Phys. **92**, 5397 (1990).